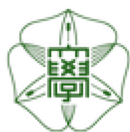

HOKKAIDO UNIVERSITY

Title	Control of plasma-CVD SiO2/InAlN interface by N2O plasma oxidation
Author(s)	Akazawa, Masamichi; Kitajima, Shouhei; Kitawaki, Yuya
Citation	Japanese Journal of Applied Physics (JJAP), 58(10), 106504 https://doi.org/10.7567/1347-4065/ab3c49
Issue Date	2019-10-01
Doc URL	http://hdl.handle.net/2115/79367
Rights	© 2019 The Japan Society of Applied Physics
Type	article (author version)
File Information	JJAP-101707_for printing.pdf

Instructions for use

Hokkaido University Collection of Scholarly and Academic Papers : HUSCAP

Control of plasma-CVD SiO_2/InAlN interface by N_2O plasma oxidation

Masamichi Akazawa*, Shouhei Kitajima and Yuya Kitawaki

Research Center for Integrated Quantum Electronics, Hokkaido University, Sapporo 060-0813, Japan

E-mail: akazawa@rciqe.hokudai.ac.jp

Control of the plasma-CVD SiO_2/InAlN interface by N_2O plasma oxidation of the InAlN surface was studied. The interface was characterized by both X-ray photoelectron spectroscopy (XPS) and capacitance–voltage measurement of metal–insulator–semiconductor (MIS) diodes. An excessively long duration of oxidation led to the deterioration of the stoichiometry of the InAlN surface and plasma oxide, resulting in a high density of interface states in the completed MIS diodes. Meanwhile, the surface-localized oxygen deficiency in the plasma oxide layer was observed by XPS. The intensity ratio of the oxygen-deficient component to the fully oxidized component in the O 1s spectrum decreased with increasing oxidation duration. Consequently, there was an optimum oxidation duration. The interface state density was reduced by almost one order in the case of plasma oxidation for an appropriate duration compared with the case of the direct deposition of SiO_2 onto InAlN.

1. Introduction

GaN has attracted much attention as a material for developing power electronics because of its wide band gap, high saturation electron velocity, high breakdown field, and good thermal conductivity.[1] One of the advantages of III-nitrides is their feasibility for constructing excellent heterostructures.[1] As an application to high-frequency power devices, AlGaN/GaN heterostructures providing a high-mobility and high-density two-dimensional electron gas (2DEG) are used to construct high-electron-mobility transistors (HEMTs). $In_xAl_{1-x}N$, which achieves lattice matching to GaN when $x = 0.17 – 0.18$, is a promising alloy for HEMT application because it can provide a higher-density 2DEG[2] owing to its high-density spontaneous polarization[3] and large conduction band offset[4], ΔE_C, with a large band gap.[5] Actually, a 2DEG density higher than 2×10^{13} cm^{-2} has been reported.[6–11] However, InAlN has the drawback of a high leakage current[12] owing to the high internal electric field resulting from the high spontaneous polarization.[13] Therefore, the use of an insulator for the gate structure is necessary. So far, several insulators, *i.e.*, Al_2O_3[12, 14–18], ZrO_2[15, 19, 20], $GdScO_3$[15], HfO_2[19], SiO_2[21], plasma oxides[22–26], and thermal oxides[27, 28], have been used to construct insulated gate HEMTs or metal–insulator–semiconductor (MIS) HEMTs. Among these insulators, SiO_2 has the widest band gap, achieving a large ΔE_C with InAlN lattice-matched to GaN. Since the insulator/semiconductor interface is generally characterized by the presence of interface states, which deteriorate the device performance, it is desirable to establish a method of controlling the SiO_2/InAlN interface.

In our previous work[29], we reported that N_2O plasma oxidation of an InAlN surface is a promising method of reducing the interface state density D_{it} at the SiO_2/InAlN interface. However, the optimum conditions for surface oxidation and the mechanism underlying the reduction in D_{it} have not been clarified. Recently, plasma oxidation of the III-nitride surface has been reported to be an excellent method of achieving surface passivation of AlGaN/GaN HEMTs.[30] In addition, the existence of an ultrathin epitaxial crystalline intermediate Ga_2O_3 layer at the plasma-CVD SiO_2/GaN interface has been reported, suggesting that the initial oxidation of the GaN surface leads to good interfacial properties.[31] These results indicate that the properties of the native oxide/III-nitride interface formed by plasma oxidation are excellent. However, the reason why the plasma-induced damage does not deteriorate the interface properties is unclear. Generally, ion attacks cause plasma damage at the sample

surface, resulting in interface disorder with random changes in the connection, length, and angle of the chemical bonds at the interface. The direct deposition of SiO_2 onto an InAlN surface by plasma CVD leads to the formation of an uncontrolled oxide layer, resulting in the generation of interface states.[29] On the other hand, successful control of the insulator/AlGaN interface by N_2O radical treatment while excluding ion attacks has been reported.[32] Therefore, an excellent native oxide/III-nitride interface can be formed only when plasma oxidation is performed appropriately. To realize this, the mechanism of formation of an excellent native oxide/III-nitride interface by plasma oxidation should be investigated.

In our very recent work[33], we reported that inserting a 0.5-nm-thick Al_2O_3 interlayer formed by atomic layer deposition (ALD) at a plasma-CVD SiO_2/InAlN interface reduces D_{it} efficiently. On the basis of X-ray photoelectron spectroscopy (XPS) results, it has been clarified that the native oxide is formed beneath the ultrathin Al_2O_3 interlayer. Therefore, the reduction in D_{it} should have been achieved by forming an excellent native oxide/InAlN interface with ion attacks blocked by the ultrathin Al_2O_3 interlayer during plasma CVD. There is a possibility that the native oxide layer grown by plasma oxidation can automatically block ion attacks at the interface.

In this work, the control of the plasma-CVD SiO_2/InAlN interface by N_2O plasma oxidation of the InAlN surface prior to SiO_2 deposition was investigated. On the basis of XPS results, the oxide growth rate, stoichiometry of the InAlN surface and plasma oxide, and oxygen deficiency in the plasma oxide were analyzed. From the results of capacitance–voltage (*C*–*V*) measurement of MIS diodes combined with simulation results, D_{it} was extracted. An appropriate duration of plasma oxidation led to a reduction in D_{it} compared with the case of the direct deposition of SiO_2 by plasma CVD, whereas a very long duration of oxidation resulted in an increase in D_{it}. The mechanism of D_{it} reduction at the optimum duration is discussed on the basis of the combined results of XPS and electrical measurement.

2. Experimental procedure

For electrical measurements, MIS diodes, as shown in Fig. 1, were fabricated as follows. A Si-doped InAlN layer was grown by metal organic vapor phase epitaxy (MOVPE) on

sapphire substrates via a GaN buffer layer. The carrier concentration *n* of the InAlN layer was adjusted to 1–3×10^{18} cm^{-3} and the thickness was 160 nm, which enabled us to characterize the samples as ordinary MIS diodes without considering the 2DEG that was located much deeper than the depletion layer edge. (Although we have not performed any special characterizations, the quality of the 160-nm-thick InAlN epitaxial layer was satisfactory for use in a MIS structure to characterize insulator-semiconductor interfaces by the *C*–*V* method and to compare the effects of fabrication process.) Chemical treatment was carried out using buffered hydrofluoric acid (HF) solution (BHF, NH_4F:HF=5:1) to remove the surface oxide. A 20-nm-thick SiN layer to protect the InAlN surface during ohmic annealing was deposited by electron cyclotron resonance plasma CVD at 270 ºC with 100 W plasma power using a N_2 and SiH_4/Ar gas mixture. After photolithography and partial removal of SiN using BHF, a Ti (20 nm; bottom)/Al (50 nm)/Ni (20 nm)/Au (50 nm; topmost) ohmic contact was formed as a large pad perforated with a periodic-hole array. Subsequently, the sample with the SiN surface protection layer was annealed at 850 ºC for 1 min. After annealing, the SiN layer was removed using the BHF solution. Then the sample surface was oxidized using N_2O RF plasma at 20 W plasma power, a substrate temperature of 300 ºC, and a pressure of 28 Pa in a N_2O flow of 27 sccm. The durations of plasma oxidation were set at 30 s, 1 min, and 3 min. For comparison, a sample without plasma oxidation was also fabricated. SiO_2 was deposited by RF plasma CVD at 300 ºC and 30 W plasma power using a N_2O and SiH_4/Ar gas mixture. The thickness of the SiO_2 layer was in the range of 21–25 nm. Finally, a Ni (20 nm, lower)/Au (50 nm, upper) circular gate electrode was formed at the center of the hole of the ohmic contact pad to complete the MIS structure.

The plasma oxide/InAlN interface was examined by XPS using a sample with an ultrathin plasma oxide layer formed on an undoped 30-nm-thick InAlN layer grown by MOVPE on a sapphire substrate via a 2-μm-thick GaN buffer layer. A monochromated Al-*K*α X-ray source (1486.6 eV) was used. The charge-up error in binding energy was calibrated by setting the C 1s spectral peak to 285.0 eV.

3. Results and discussion

The XPS In 3d, N 1s, and Al 2p spectra observed at the photoelectron take-off angle θ of

45° for the InAlN surface after plasma oxidation for various durations are shown in Fig. 2. Oxide components are observed clearly in the Al 2p and In 3d spectra, whereas no oxide component can be seen in the N 1s spectrum. The shape of the N 1s spectrum obtained from the InAlN surface after plasma oxidation coincided with that of the HF-treated InAlN surface. Therefore, a native oxide layer without oxynitride components was formed by this plasma oxidation. It can be seen that the intensity ratio R_I of the oxide component to the InAlN component increased with the oxidation duration in both the In 3d and Al 2p spectra. This indicates that the thickness of the surface oxide layer increased with the oxidation duration. Here, the oxide thickness can be estimated from the obtained Al 2p spectrum as follows. The integrated intensity $I_{CL\ InAlN}$ of a core-level spectrum from the InAlN layer decays with increasing plasma oxide thickness d_{POX} as[34)]

$$I_{CL\ InAlN} = I_{0CL\ InAlN} \exp(-\frac{d_{POX}}{\lambda}), \quad (1)$$

where $I_{0CL\ InAlN}$ indicates $I_{CL\ InAlN}$ with $d_{POX} = 0$, and λ is the escape depth of photoelectrons given by

$$\lambda = \lambda_0 sin\theta, \quad (2)$$

where λ_0 is the inelastic mean free path of photoelectrons. Using λ_0 determined by the theoretical calculation[35, 36)], we calculated λ at $\theta = 45°$ to be 1.7, 1.8, and 2.2 nm for In 3d, N 1s, and Al 2p, respectively. On the other hand, the integrated intensity $I_{CL\ POX}$ of the same core-level spectrum from the plasma oxide layer increases with an increase in d_{POX} as[34)]

$$I_{CL\ POX} = I_{0CL\ POX} \left\{1 - \exp(-\frac{d_{POX}}{\lambda})\right\}, \quad (3)$$

where $I_{0CL\ POX}$ indicates $I_{CL\ POX}$ with an infinite or sufficiently large d_{POX}. Consequently, for the spectra obtained from the oxidized InAlN surface, R_I is given by[34)]

$$R_I = \left(\frac{I_{0CL\,POX}}{I_{0CL\,InAlN}}\right)\frac{1-exp\left(-\frac{d_{POX}}{\lambda}\right)}{exp\left(-\frac{d_{POX}}{\lambda}\right)}. \quad (4)$$

Using this equation, d_{POX} was derived from R_I. Here, we used the Al 2p spectrum because the ratio $I_{0CL\ POX}/I_{0CL\ InAlN}$ can be extracted from the Al_2O_3/InAlN structures formed by ALD, with the assumption that the molar fraction of Al oxide in the native oxide layer is equal to that of AlN in InAlN. The extracted d_{POX} is plotted as a function of oxidation duration in Fig. 3. It can be seen that d_{POX} increases with the oxidation duration. The dashed line in Fig. 3 shows an example fitting line calculated with the Deal–Grove model[37] given by

$$d_{POX} = \frac{A}{2}\left\{\left(1+\frac{t+\tau}{A^2/4B}\right)^{1/2} - 1\right\}, \quad (5)$$

where A and B are used as fitting parameters (an explanation of their physical meaning is omitted here) and τ is a parameter related to the initial thickness and was set to 0.

Figure 4 shows the integrated intensity $I_{CL\ InAlN}$ as a function of the extracted d_{POX} for the In 3d, N 1s, and Al 2p spectra. The dashed lines indicate fitting curves given by Eq. (1). Although reasonable fitting within the experimental error can be seen for N 1s and Al 2p, the discrepancy between the estimated intensity and the measured intensity is considerable for In 3d at the largest d_{POX}. It is highly likely that the stoichiometry at the InAlN surface was deteriorated by the oxidation for 3 min. In addition, the stoichiometry of the plasma oxide layer was also deteriorated by 3 min oxidation. The intensity ratio R_I for the Al 2p and In 3d core-level spectra is plotted as a function of d_{POX} in Fig. 5, where the solid and dashed lines are fitting lines calculated by Eq. (4). It can be seen that the measured R_I for In 3d deviates from the estimation at the largest d_{POX}, being much lower than the estimated value. This result indicates a deficit of the In component in the plasma oxide layer for the sample with 3 min oxidation. On the basis of these results, it is concluded that an excessively long duration of oxidation leads to deterioration of the stoichiometry of the InAlN surface and plasma oxide. Presumably, the In component at the InAlN surface is more difficult to oxidize compared with Al component, or the Al component is more easily oxidized than the In component, when the oxidation duration is too long. This phenomenon

should affect the quality of the insulator/semiconductor interface of the completed MIS diodes.

The chemical bond connection in the native oxide layer may also affect the interface quality. O1s spectra obtained at $\theta = 45^{\circ}$ for different oxidation durations are illustrated in Fig. 6(a), where the O 1s spectra are decomposed into two components, in which the In- and Al-related components are merged for each, with a chemical shift of ~1.5 eV. The lower-energy component denoted by O_I consists of In_2O_3 [38] and Al_2O_3 [39]. It is reported that the hydroxide components exhibits higher binding energy with a similar chemical shift.[38, 39] However, since the N_2O oxidation was carried out in vacuum, it is unlikely that hydroxides dominate in the higher-energy component denoted by O_{II}. Alternatively, it is highly likely that the higher-energy component is mainly composed of the oxygen-deficient region including dangling bonds[40–42]. The spatial location of this region was clarified by angle-resolved XPS, as shown in Fig. 6(b), where O 1s spectra observed at $\theta = 15$, 45, and 90° are plotted for the 1-min-oxidized sample. It can be clearly seen that the intensity of the O_{II} component increased as θ decreased. Since a decrease in θ makes the analysis more surface-sensitive; this result indicates that the oxygen-deficient region was localized at the topmost surface of the native oxide layer. On the other hand, in Fig. 6(a), it can be seen that the ratio of the integrated intensity of the oxygen-deficient component I_{OII} to that of the fully oxidized component I_{OI} decreased with increasing oxidation duration. This ratio (I_{OII}/I_{OI}) is plotted in Fig. 7 as a function of d_{POX}, where its almost linear decay can be seen. The effect of this tendency is discussed later.

The XPS results described above should be related to the electrical properties of the interface. It is naturally expected that the quality of the SiO_2/InAlN interface of the completed MIS diode is dependent on the native oxide/InAlN interface. One of the most important parameters concerning the interface quality is D_{it}. According to the disorder-induced gap state (DIGS) model[43], interface disorder is the origin of interface states. Since the stoichiometry of the InAlN surface and plasma oxide deteriorated in the sample with 3 min plasma oxidation, there is a possibility that interface disorder was introduced at the interface. Therefore, it is anticipated that D_{it} of the MIS diodes with 3 min plasma oxidation is high. Figure 8 shows a summary of the results of the C–V measurement at a frequency of 1 MHz, where the solid lines indicate the measured data,

the one-dot-chain lines are the calculated ideal curves, and the open circles indicate simulated curves used to fit the measured ones. For comparison, the data taken from Ref. 33 for the sample with direct SiO_2 deposition are also plotted in Fig. 8(a). The oxide thicknesses were 20 nm for direct SiO_2 deposition, 25 nm for the 30-s- and 3-min-oxidized samples, and 21 nm for the 1-min-oxidized sample. The difference in SiO_2 thickness was due to an error in thickness control. The doping density also varied among the sample owing to the unoptimized doping conditions. Nevertheless, the properties of the samples can be compared using the ideal curves, which were calculated by taking into account the difference in the conditions, as a benchmark. It can be seen that the sample with 1 min plasma oxidation exhibits the best *C*–*V* characteristic, whereas that of the sample with 3 min plasma oxidation indicates the existence of a high D_{it}. The ideal *C*–*V* curves are calculated using a previously developed simulator.[44, 45] Generally, the measured curve exhibits a voltage shift from the ideal curve. In Fig. 8, the ideal curves were shifted in the voltage axis direction to overlap with the measured *C*–*V* curves for comparison. The magnitude of this voltage shift of each ideal *C*–*V* curve is denoted by ΔV and summarized in Table I. The origin of ΔV is discussed later.

Using the same simulator, *C*–*V* curves were calculated to obtain the best fit to the measured data by taking into account the charge/discharge of interface states. The D_{it} distribution was assumed to be U-shaped on the basis of the DIGS model.[43] As a mathematical model of the D_{it} distribution, the following equation can be appropriately used to simulate the *C*–*V* curves[44, 45]:

$$D_{it}(E) = D_{it0} exp\left(\left|\frac{E-E_{CNL}}{E_{0D,0A}}\right|^{n_D,n_A}\right), \tag{6}$$

where D_{it0} is the minimum of D_{it}, E_{CNL} is the charge neutrality level, E_{0D} and n_D are the curvature factors assumed for the donorlike states below E_{CNL}, and E_{0A} and n_A are those for the acceptorlike states above E_{CNL}. E_{CNL} was assumed to be located 2.0 eV below the conduction band minimum energy, E_C[17]. Therefore, E_{0D} and n_D cannot be determined from the *C*–*V* curves of the n-type MIS diode because the response of the interface states located below E_{CNL} becomes too slow. Here, D_{it0}, E_{0A}, and n_A are used as parameters for fitting to the measured *C*–*V* curves. By fitting, we can extract the D_{it} distributions. The extracted D_{it}

distributions are summarized in Fig. 9, where the data for the sample with the direct SiO_2 deposition are taken from our previous work[33]. It can be seen that the 1-min-oxidized sample exhibited the lowest D_{it}, whereas the 3-min-oxidized sample showed the highest D_{it}. Compared with the sample without plasma oxidation, the sample with the most appropriate duration of oxidation achieved a one-order reduction in D_{it}.

In our previous work[33], we argued that ΔV is the sum of the polarization charge Q_{pol}, the fixed charge Q_f distributed at the interface and possibly in insulator, and the charge Q_{it}^{fr} owing to the frozen interface states with a long time constant compared with the speed of the bias sweep. However, using Q_{it}^{fr} determined from the D_{it} distributions extracted by the simulation, the extracted Q_f was very high even for the SiO_2/InAlN interface controlled by the Al_2O_3 interlayer in Ref. 33 and that controlled by the plasma oxide interlayer in this work, resulting in a high Q_f/q on the order of 10^{13} cm^{-2} (q is the elemental charge). Since this density seems to be too high for an excellent interface with a low D_{it}, the estimation of Q_f/q should be reappraised. Because Q_{pol}/q is as large as -2.88×10^{13} cm^{-2} [3], an estimation of Q_f/q results in a high value. There is a possibility that another type of charge compensated for Q_{pol} at the interface or the InAlN surface. One of the possible compensation charges is surface donors[46]. If this charge is taken into account, ΔV is given by

$$\Delta V = -\frac{1}{C_I}\left(Q_{pol} + Q_{SD} + Q_f + Q_{it}^{fr}\right), \tag{7}$$

where C_I is the insulator capacitance and Q_{SD} is the charge density of surface donors. Nevertheless, the exact value of Q_{SD} is unclear here. Therefore, we can only obtain an apparent fixed charge Q_{fapp} given by

$$Q_{fapp} = Q_{pol} + Q_{SD} + Q_f. \tag{8}$$

In the simulation, this Q_{fapp} and the D_{it} distribution were adjusted as parameters to fit the C–V curves. Namely, the D_{it} distribution that determined Q_{it}^{fr} was adjusted to reproduce the shape of the C–V curve, whereas Q_{fapp} was adjusted so that the simulated curve overlapped

the measured curve, resulting in the determination of ΔV given by Eq. (7). Figure 10 plots the extracted Q_{fapp}/q as a function of d_{POX}. It can be seen that Q_{fapp} increases with plasma oxide interlayer thickness. This indicates that the plasma oxide interlayer contains the bulk fixed charge, although the origin of this bulk charge is unclear at this stage.

On the basis of the results of both XPS and electrical measurements, the optimum oxidation duration was found. An excessively long duration of oxidation resulted in the deterioration of the stoichiometry of the InAlN surface and plasma oxide, which led to interface disorder that generated a high D_{it}. On the other hand, shorter durations of 30 s and 1 min resulted in low D_{it} values. The oxygen-deficient component was detected in the O 1s spectra of all samples, as shown in Fig. 6(a), although $I_{\mathrm{OII}}/I_{\mathrm{OI}}$ decreased with increasing oxidation duration as shown in Fig. 7. This means that the oxygen-deficient component existed in the native oxide layer even in the 1-min-oxidized sample with the lowest D_{it}. It seems unusual that an interface with oxygen deficiency exhibited a low D_{it}. The decrease in $I_{\mathrm{OII}}/I_{\mathrm{OI}}$ with increasing oxidation duration in Fig. 7 was likely to be due to the increase in thickness, which led to a decrease in the ratio of the surface-localized component to the oxide-bulk component. There is a possibility that the oxygen-deficient region is the product of plasma damage that introduces defects and/or dangling bonds at the topmost surface of the native oxide layer, whereas a plasma oxide layer without oxygen deficiency or any defects exists at the native oxide/InAlN interface. That is, it is highly likely that plasma oxide prevents the native oxide/InAlN interface from ion attacks by itself. Considering that the lowest D_{it} was observed in 1-min-oxidized sample, the amount of the surface-localized $\mathrm{O_{II}}$ component might have been reduced after SiO_2 deposition owing to chemical bonding at the SiO_2/native oxide interface, achieving a reduction in D_{it} in the completed MIS structure. Nevertheless, since residual defects might have existed in the vicinity of the SiO_2/native oxide interface and affected the interface states at the native oxide/InAlN interface by tunneling, the thickness of the native oxide layer should be sufficiently large to reduce D_{it} by separating these interfaces. The slight increase in D_{it} of the 30-s-oxidized sample possibly resulted from its slightly smaller plasma oxide interlayer thickness, or higher tunneling probability, than that of the 1-min-oxidized sample. Consequently, a tradeoff exists between maintaining the stoichiometry of the InAlN surface and plasma oxide and separating the two interfaces, which results in an optimum oxidation duration.

4. Conclusions

Control of the plasma-CVD SiO_2/InAlN interface by N_2O plasma oxidation of the InAlN surface was studied. The interface was characterized by both XPS and *C*–*V* measurement of MIS diodes subjected to 30 s, 1 min, and 3 min interface oxidation. The 3 min oxidation led to the deterioration of the stoichiometry of the InAlN surface and plasma oxide, resulting in a high density of interface states in the completed MIS diode. On the other hand, the lowest D_{it}, which was almost one order lower than that of the sample with the direct deposition of SiO_2, was achieved by 1 min plasma oxidation. The surface-localized oxygen-deficient component in the plasma native oxide layer was observed in the XPS O 1s spectrum. The intensity ratio of the oxygen-deficient component to the fully oxidized component decreased with increasing the oxidation duration and resultant oxide thickness. A slight increase in D_{it} was obtained for the 30-s-oxidized sample compared with the 1-min-oxidized sample, which is possibly because of the slightly smaller native oxide thickness.

Acknowledgments

This work was supported by JSPS KAKENHI Grant Number JP15K04672 and JP16H06421.

References

1) D. Ueda, in *Power GaN Devices*, eds. M. Meneghini, G. Meneghesso, and E. Zanoni (Springer, Berlin, 2017) Chap. 1.
2) J. Kuzmík, IEEE Electron. Device Lett. **22**, 510 (2001).
3) O. Ambacher, R. Dimitrov, M. Stutzmann, B. E. Foutz, M. J. Murphy, J. A. Smart, J. R. Shealy, N. G. Weimann, K. Chu, M. Chumbes, B. Green, A. J. Sierakowski, W. J. Schaff and L. F. Eastman, Phys. Status Solidi B **216**, 381 (1999).
4) W. Walukiewicz, S. X. Li, J. Wu, K. M. Yu, J. W. Ager III, E. E. Haller, H. Lu, and W. J. Schaff, J. Cryst. Growth **269**, 119 (2004).
5) R. E. Jones, R. Broesler, K. M. Yu, J. W. Ager III, E. E. Haller, W. Walukiewicz, X. Chen and W. J. Schaff, J. Appl. Phys. **104**, 123501 (2008).
6) M. Higashiwaki and T. Matsui, Jpn. J. Appl. Phys. **43**, L768 (2004).
7) J. Kuzmík, A. Kostopoulos, G. Konstantinidis, J.-F. Carlin, A. Georgakilas and D. Pogany, IEEE Electron. Device Lett. **53**, 422 (2006).
8) M. Gonschorek, J.-F. Carlin, E. Feltin, M. A. Py and N. Grandjean, Appl. Phys. Lett. **89**, 062106 (2006).
9) J. Xie, X. Ni, M. Wu, J. H. Leach, Ü. Özgür and H. Morkoç, Appl. Phys. Lett. **91**, 132116 (2007).
10) M. Gonschorek, J.-F. Carlin, E. Feltin, M. A. Py, N. Grandjean, V. Darakchieva, B. Monemar, M. Lorenz and G. Ramn, J. Appl. Phys. **103**, 093714 (2008).
11) L. Ardaravičius, M. Ramonas, J. Liberis, O. Kiprijanovič, A. Matulionis, J. Xie, M. Wu, J. H. Leach and H. Morkoç, J. Appl. Phys. **106**, 073708 (2009).
12) G. Pozzovivo, J. Kuzmík, S. Golka, W. Schrenk, G. Strasser, D. Pogany, K. Ĉiĉo, M. Ťapajna, K. Fröhlich, J.-F. Carlin, M. Gonschorek, E. Feltin and N. Grandjean, Appl. Phys. Lett. **91**, 043509 (2007).
13) J. Kotani Atsushi Yamada, Tetsuro Ishiguro, Shuichi Tomabechi and Norikazu Nakamura, Appl. Phys. Lett. **108**, 152109 (2016).
14) K. Čičo, J. Kuzmík, J. Liday, K. Hušeková, G. Pozzovivo, J.-F. Carlin, N. Grandjean, D. Pogany, P. Vogrinčič and K. Fröhlich, J. Vac. Sci. Technol. **B27**, 218 (2009).
15) K. Čičo, K. Hušeková, M. Ťapajna, D. Gregušová, R. Stoklas, J. Kuzmík, J.-F. Carlin, N. Grandjean, D. Pogany and K. Fröhlich, J. Vac. Sci. Technol. **B29**, 01A808 (2011).

16) M. Ťapajna, K. Čičo, J. Kuzmík, D. Pogany, G. Pozzovivo, G. Strasser, J.-F. Carlin, N. Grandjean and K. Fröhlich, Semicond. Sci. Technol. **24**, 035008 (2009).
17) M. Akazawa, M. Chiba and T. Nakano, Appl. Phys Lett. **102**, 231605 (2013).
18) S. Ozaki, K. Makiyama, T. Ohki, N. Okamoto, S. Kaneki, K. Nishiguchi, N. Hara, and T. Hashizume, Appl. Phys. Express **10**, 061001 (2017).
19) J. Kuzmík, G. Pozzovivo, S. Abermann, J.-F. Carlin, M. Gonschorek, E. Feltin, N. Grandjean, E. Bertagnolli, G. Strasser and D. Pogany, IEEE Trans. Electron Devices **55**, 937 (2008).
20) P. Kordoš, R. Stoklas, D. Gregušová, K. Hušeková, J.-F. Carlin and N. Grandjean, Appl. Phys. Lett. **102**, 063502 (2013).
21) M. Lachab, M. Sultana, Q. Fareed, F. Husna, V. Adivarahan and A. Khan, J. Phys. D: Appl. Phys. **47**, 135108 (2014).
22) D. S. Lee, X. Gao, S. Guo and T. Palacios, IEEE Electron Device Lett. **32**, 617 (2011).
23) D. S. Lee, J. W. Chung, H. Wang, X. Gao, S. Guo, P. Fay and T. Palacios, IEEE Electron Device Lett. **32**, 755 (2011).
24) D. S. Lee, X. Gao, S. Guo, D. Kopp, P. Fay and T. Palacios, IEEE Electron Device Lett. **32**, 1525 (2011).
25) Y. Yue, Z. Hu, J. Guo, B. Sensale-Rodriguez, G. Li, R. Wang, F. Faria, T. Fang, B. Song, X. Gao, S. Guo, T. Kosel, G. Sinder, P. Fay, D. Jena and H. Xing, IEEE Electron Device Lett. **33**, 988 (2012).
26) Y. Yue, Z. Hu, J. Guo, B. Sensale-Rodriguez, G. Li, R. Wang, F. Faria, B. Song, X. Gao, S. Guo, T. Kosel, G. Sinder, P. Fay, D. Jena and H. Xing, Jpn. J. Appl. Phys. **52**, 08JN14 (2013).
27) M. Eickelkamp, M. Weingarten, L. Rahimzadeh Khoshroo, N. Katteniss, H. Behmenburg, M.Heuken, D. Donoval, A. Chvála, P. Kordoš, H. Kalisch and A. Vescan, J. Appl. Phys. **110**, 084501 (2011).
28) S. Ozaki, K. Makiyama, T. Ohki, Y. Kamada, M. Sato, Y. Niida, N. Okamoto and K. Joshin, Phys. Status Solidi A **213**, 1259 (2015).
29) M. Akazawa and A. Seino, Phys. Status Solidi B **254**, 1600691 (2017).
30) M. Mi, X.-H. Ma, L. Yang, Y. Lu, B. Hou, J. Zhu, M. Zhang, H.-S. Zhang, Q. Zhu, L.-A. Yang, and Y. Hao, IEEE Trans. Electron. Devices **64**, 4875 (2017).

31) K. Mitsuishi, K. Kimoto, Y. Irokawa, T. Suzuki, K. Yuge, T. Nabatame, S. Takashima, K. Ueno, M. Edo, K. Nakagawa, and Y. Koide, Jpn. J. Appl. Phys. **56**, 110312 (2017).
32) Y. Hori, Z. Yatabe, and T. Hashizume, J. Appl. Phys. **114**, 244503 (2013).
33) M. Akazawa and S. Kitajima, Jpn. J. Appl. Phys. **58**, SIIB06 (2019).
34) D. Briggs and M. P. Seah, *Practical Surface Analysis by Auger and X-ray Photoelectron Spectroscopy* (John Wiley & Sons Ltd., Sussex, 1983) Chap. 4.
35) S. Tanuma, C. J. Powell, and D. R. Penn, Surf. Interface Anal. **17**, 927 (1991).
36) S. Tanuma, C. J. Powell, and D. R. Penn, Surf. Interface Anal. **21**,165 (1993).
37) E. H. Nicollian and J. R. Brews, *MOS (Metal Oxide Semiconductor) Physics and Technology* (John Wiley & Sons, Inc., Hoboken, 1981) Chap. 13.
38) N. Asai, Y. Inoue, H. Sugimura, and O. Takai, J. Electrochem. Soc. **146**, 2365 (1999).
39) M. R. Alexander, G. E. Thompson and G. Beamson, Surf. Interface Anal. **29,** 468 (2000).
40) J. S. Kim, P. K. H. Ho, D. S. Thomas, R. H. Friend, F. Cacialli, G.-W. Bao, and S. F. Y. Li, Chem. Phys. Lett. **315**, 307 (1999).
41) A. Thøgersen, M. Rein, E. Monakhov, J. Mayandi, and S. Diplas, J. Appl. Phys. **109**, 113532 (2011).
42) Y. Gao, J. Lu, J. Zhang, and X. Li, J. Alloys Compd. **646**, 675 (2015).
43) H. Hasegawa and H. Ohno, J. Vac. Sci. & Technol. B **4**, 1130 (1986).
44) M. Miczek, C. Mizue, T. Hashizume and B. Adamowicz, J. Appl. Phys. **103**, 104510 (2008).
45) M. Miczek, B. Adamowicz, C. Mizue and T. Hashizume, Jpn. J. Appl. Phys. **48**, 04C092 (2009).
46) M. Ťapajna and J. KuzmíK, Appl. Phys. Lett. 100, 113509 (2012).

Figure Captions

Fig. 1. Structure of tested MIS diode.

Fig. 2. XPS spectra obtained from InAlN surface after plasma oxidation, *i.e.*, In 3d, N 1s, and Al 2p spectra for oxidation durations of 30 s, 1 min, and 3 min.

Fig. 3. Plot of the thickness of the oxide layer formed by plasma oxidation, derived from the intensity ratio of the oxide component to the InAlN component in the Al 2p spectrum, as a function of oxidation duration.

Fig. 4. Plots of integrated intensity $I_{\mathrm{CL\ InAlN}}$ as a function of d_{POX}. The dashed lines are fitting lines calculated by Eq. (1) assuming λ to be 1.7, 1.8, and 2.2 nm for In 3d, N 1s, and Al 2p, respectively.

Fig. 5. Plots of integrated intensity ratio R_{I} of oxide component to InAlN component as a function of d_{POX} for Al 2p and In 3d core level spectra. The dashed and solid lines indicate the theoretical estimation calculated by Eq. (4) for Al 2p and In 3d, respectively.

Fig. 6. (a) O 1s spectra obtained at $\theta = 45^{\circ}$ for oxidation durations of 30 s, 1 min, and 3 min. (b) O 1s spectra obtained by angle-resolved XPS for the 1-min-oxidized InAlN surface.

Fig. 7. Plot of intensity ratio $I_{\mathrm{OII}}/I_{\mathrm{OI}}$ as a function of d_{POX}.

Fig. 8. *C–V* curves measured at 1 MHz for fabricated MIS diodes (solid lines) with the calculated ideal curves (one-dot-chain lines) and the simulated curves (open circles). (a) Direct SiO_2 deposition (Data are taken from Ref. 33). (b) N_2O oxidation for 30 s. (c) N_2O oxidation for 1 min. (d) N_2O oxidation for 3 min.

Fig. 9. Summary of the D_{it} distributions assumed in the simulation for the best fit to the measured *C–V* curves. The data for the sample with direct SiO_2 deposition are taken from

Ref. 33.

Fig. 10. Plot of Q_{fapp}/q as a function of plasma oxide interlayer thickness. The solid circles indicate Q_{fapp}/q estimated for the MIS diodes, and the solid line is the fitting line to the solid circles.

Table I. Summary of ΔV for the ideal curves.

Oxidation duration [min]	ΔV [V]
0	3.2
0.5	2.8
1.0	2.1
3.0	2.8

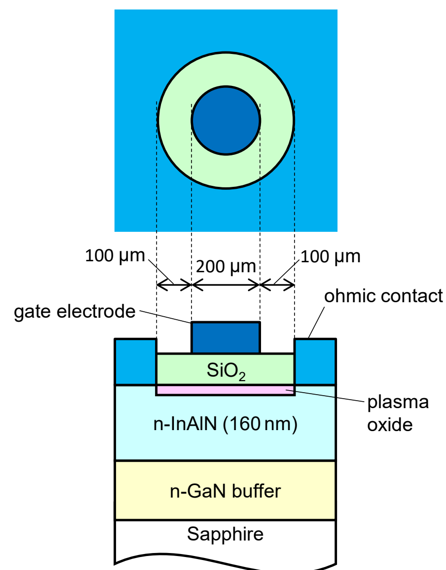

Fig. 1

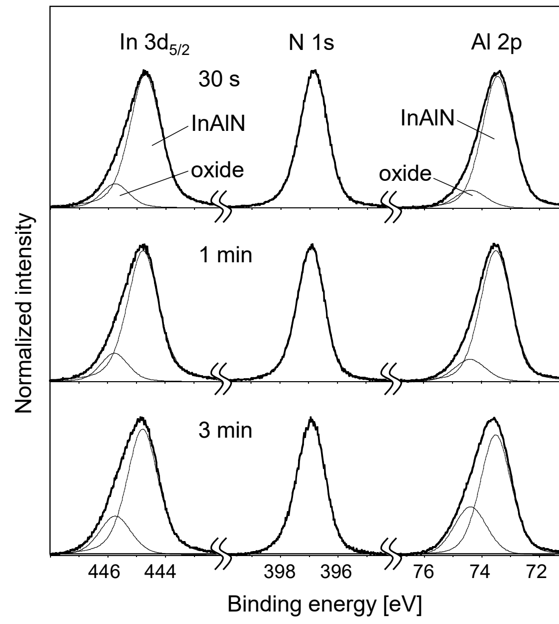

Fig. 2

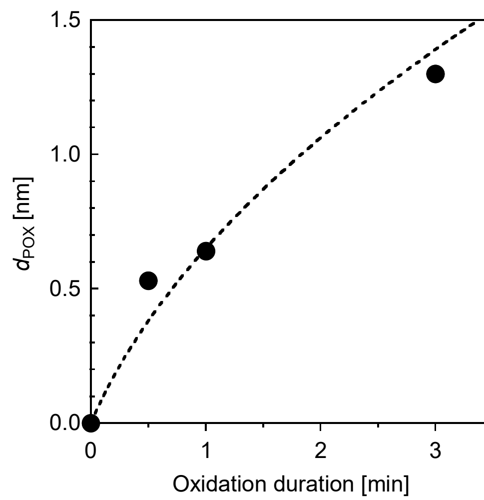

Fig. 3

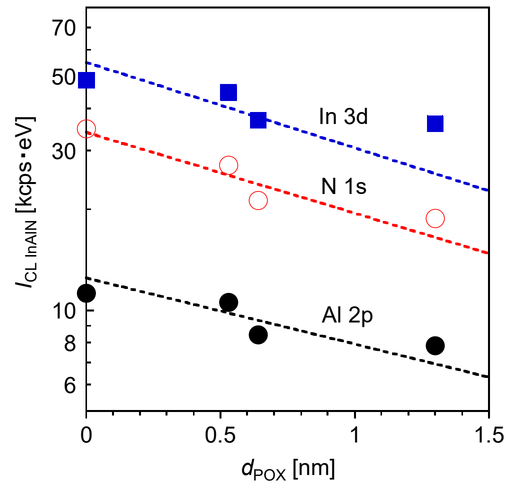

Fig. 4

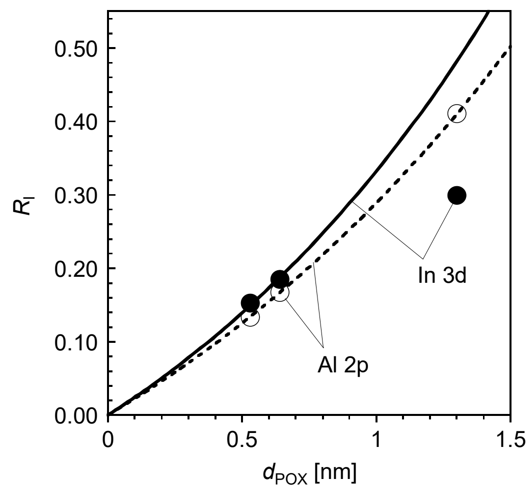

Fig. 5

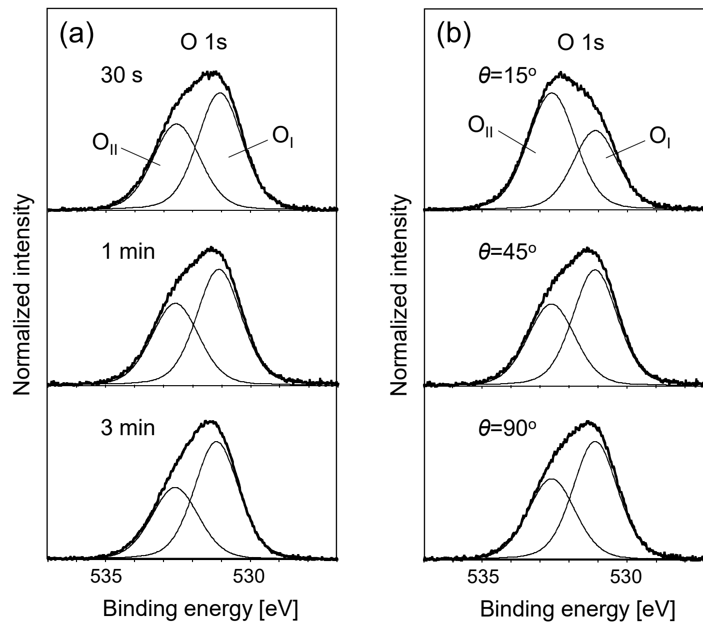

Fig. 6

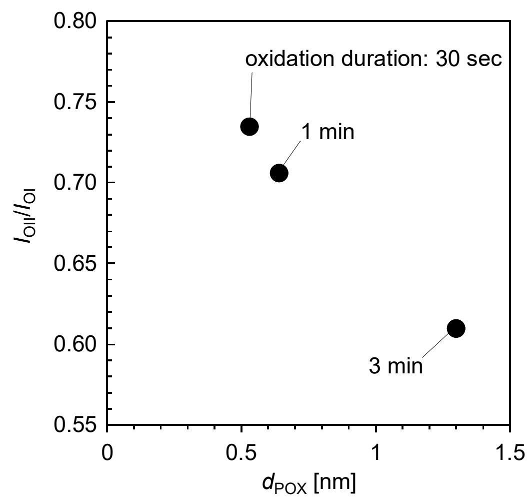

Fig. 7

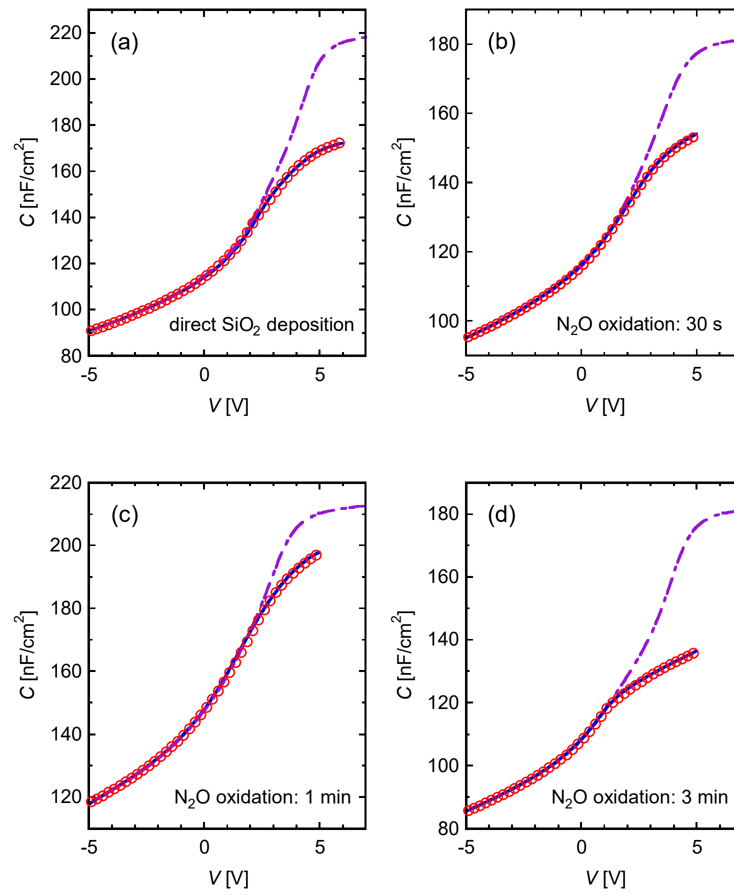

Fig. 8

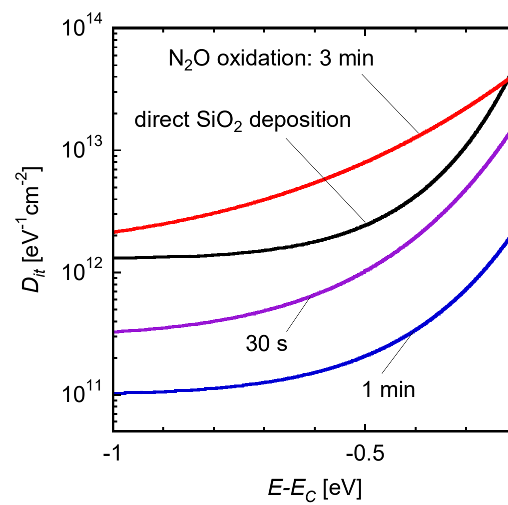

Fig. 9

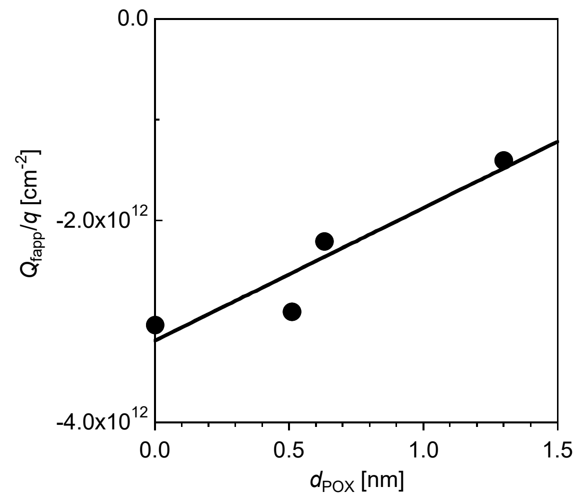

Fig. 10